FULL PAPER

ADVANCED FUNCTIONAL MATERIALS

DOI: 10.1002/adfm.200700191

A Novel Fluorene-Triphenylamine Hybrid That is a Highly Efficient Host Material for Blue-, Green-, and Red-Light-Emitting Electrophosphorescent Devices**

By *Ping-I Shih*, *Chen-Han Chien*, *Fang-Iy Wu*, and *Ching-Fong Shu**

TFTPA (tris[4-(9-phenylfluoren-9-yl)phenyl]amine), a novel host material that contains a triphenylamine core and three 9-phenyl-9-fluorenyl peripheries, was effectively synthesized through a Friedel-Crafts-type substitution reaction. Owing to the presence of its sterically bulky 9-phenyl-9-fluorenyl groups, **TFTPA** exhibits a high glass transition temperature (186 °C) and is morphologically and electrochemically stable. In addition, as demonstrated from atomic force microscopy measurements, the aggregation of the triplet iridium dopant is significantly diminished in the **TFTPA** host, resulting in a highly efficient full-color phosphorescence. The performance of **TFTPA**-based devices is far superior to those of the corresponding mCP- or CBP-based devices, particularly in blue- and red-emitting electrophosphorescent device systems. The efficiency of the FIrpic-based blue-emitting device reached 12 % (26 cd A^{-1}) and 18 lm W^{-1} at a practical brightness of 100 cd m^{-2}; the $Ir(piq)_2$acac-based red-emitting device exhibited an extremely low turn-on voltage (2.6 V) and a threefold enhancement in device efficiency (9.0 lm W^{-1}) relative to those of reference devices based on the CBP host material.

1. Introduction

Organic light-emitting diodes (OLEDs) are being investigated widely for their potential applications within full-color flat-panel displays.[1] Among these devices, the use of phosphorescent emitters has stimulated the development of efficient heavy metal-containing electroluminescent guest systems.[2,3] The ability of these phosphorescent dyes to harvest both singlet and triplet excitons can, theoretically, increase the internal efficiency of devices up to 100 %.[4–6] In these phosphorescent OLEDs, the triplet emitters are normally used as emitting guests in a host material to reduce the self-quenching associated with the relatively long excited state lifetimes of triplet emitters and triplet-triplet annihilation; consequently, the choice of host materials is of vital importance for the preparation of efficient phosphorescent OLEDs. The carbazole-based molecule 4,4′-bis(9-carbazolyl)-2,2′-biphenyl (CBP) [glass transition temperature (T_g) = 62 °C][7] has been used frequently as a host material in green- and red-emitting phosphorescent devices—even though the triplet energy of CBP (2.56 eV) is lower than that of the general blue triplet emitters (> 2.62 eV), resulting in an inefficient energy transfer from host to guest.[8] To overcome this obstacle, structurally modified host molecules, such as 1,3-bis(9-carbazolyl)benzene (mCP), which has a higher-value E_T (2.90 eV), have typically been utilized to fabricate blue-emitting OLEDs; bis[(4′,6′-difluorophenyl)pyridinato-N,$C^{2'}$]iridium(III) picolinate (FIrpic; E_T = 2.65 eV) is the most popular choice for the dopant.[8] Although mCP possesses a suitable triplet energy, its relatively low thermal and morphological stability [glass transition temperature (T_g) = 60 °C][7] may hinder its application as a host material in OLEDs. In attempts to overcome these problems and realize efficient blue-emitting devices, several carbazole derivatives have been prepared, but their syntheses often suffer from drawbacks such as complicated reaction conditions and moderate to low yields.[9,10]

In this paper, we describe the facile synthesis of a novel fluorene/triarylamine hybrid (tris[4-(9-phenylfluoren-9-yl)phenyl]amine, **TFTPA**)—through a simple one-step reaction from commercially available starting materials—and its superior characteristics that make it suitable for use as a host material in full-color phosphorescent devices. The design of **TFTPA** was based on triphenylamine and fluorene both possessing large triplet energy gaps (3.04 and 2.95 eV, respectively).[11,12] Because the triphenylamine unit is connected to the sp^3-hybridized carbon atom at the C-9 position of the fluorene moiety, which serves as a spacer to block extended π-conjugation,[13] the conjugation length and triplet energy of each individual building block in the resulting composite should remain essentially unperturbed. In addition, the 3D cardo structure of substituted fluorene derivative should improve the system's rigidity and hinder any unwanted aromatic π-stacking interactions, resulting in an amorphous material possessing enhanced morphological stability. More importantly, we expected that the

[*] Prof. C.-F. Shu, P.-I. Shih, C.-H. Chien, Dr. F.-I. Wu
Department of Applied Chemistry, National Chiao Tung University
Hsinchu, 300 Taiwan (ROC)
E-mail: shu@cc.nctu.edu.tw

[**] We thank the MOE ATU Program and the National Science Council for financial support. Our special thanks go to Professor C.-H. Cheng for his support and cooperation during the preparation and characterization of the light-emitting devices.

ADVANCED FUNCTIONAL MATERIALS

sterically hindered phenyl-substituted fluorene peripheries of **TFTPA** would alleviate the triplet-triplet annihilation and concentration quenching arising from strong bimolecular interactions of the phosphor at high doping levels,[14,15] leading to highly efficient phosphorescent devices.

2. Results and Discussion

2.1. Synthesis

As illustrated in Scheme 1, the acid promoted Friedel-Crafts-type substitution reaction of triphenylamine (**TPA**) with 3 equivalents of 9-phenyl-9-fluorenol in 1,4-dioxane solution in the presence of trifluoromethanesulfonic acid at 80 °C for 3 h

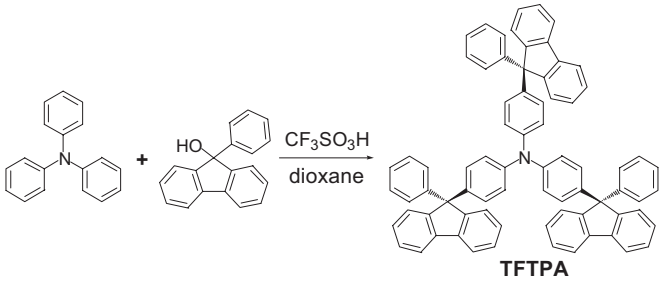

Scheme 1. Synthesis of **TFTPA**

afforded **TFTPA** as a crude white product. This reaction proceeded smoothly through protonation of 9-phenyl-9-fluorenol, generating a transitory carbocation,[16–18] which in turn underwent Friedel–Crafts-type electrophilic substitution very efficiently and exclusively at the electron-rich para carbon atom(s) of the **TPA** phenyl groups. After cooling, the precipitate was filtered, washed with acetone, and purified through repeated vacuum sublimation to give pure **TFTPA** (72 %). It is noteworthy that this overall yield is much higher than that reported for other effective host materials, and that our present preparation method was performed under mild reaction conditions in the absence of expensive noble-metal catalysts. Moreover, because this protocol does not require chromatographic purification of the product, it seems to be suitable for large-scale production. The product **TFTPA** was characterized using ^{1}H and ^{13}C NMR spectroscopy, elemental analysis, and high-resolution mass spectrometry.

2.2. Properties

TFTPA exhibits very high thermal stability; thermogravimetric analysis (TGA) performed under a nitrogen atmosphere revealed that the onset decomposition temperature was 430 °C, followed by 5 % weight loss at 491 °C. During differential scanning calorimetry (DSC) measurements, **TFTPA** existed in a glassy state after rapid cooling from the melt (at ca. 400 °C) and underwent a glass transition at a relatively high temperature (T_g = 186 °C). The higher value of T_g for **TFTPA**, with respect to those of mCP (T_g = 60 °C) and other carbazole analogues,[7,9,10] is presumably the result of its higher molecular weight and the presence of its rigid fluorene peripheries.[19] Consequently, **TFTPA** forms an amorphous glass that is more stable than that of common host materials and, therefore, it is more promising—in terms of its thermal stability—for application within OLEDs. Figure 1 displays the TGA thermogram and DSC curve of **TFTPA**. Because of its excellent thermal and morphological stability, we could use vacuum deposition to prepare homogeneous, stable amorphous thin films of **TFTPA**. Atomic force microscopy (AFM) measurements indicated that

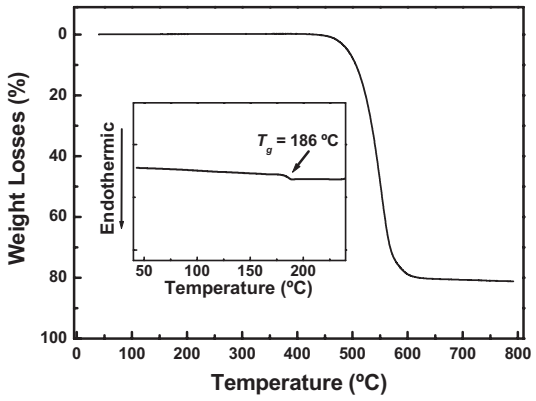

Figure 1. TGA thermogram of **TFTPA** recorded at a heating rate of 20 °C min^{-1}. Inset: DSC trace of **TFTPA** recorded at a heating rate of 20 °C min^{-1}.

an evaporated film of **TFTPA** possessed a uniform surface that did not undergo any morphological changes when annealed at 120 °C for 40 h under a nitrogen atmosphere; the root-mean-square surface roughness of this annealed film was very narrow (only 0.32 nm). On the other hand, annealing of a film of mCP, of which the root-mean-square surface roughness was 0.33 nm before annealing, induced the degradation of the surface morphology.

We used cyclic voltammetry, with ferrocene as the internal standard, to examine the electrochemical behavior of **TFTPA**. As indicated in the inset of Figure 2, **TFTPA** exhibits a reversible oxidation process with an oxidation potential ($E_{1/2}$) of 0.46 V. In contrast, the oxidation process of the pristine **TPA** is irreversible; this phenomenon can be attributed to the electrochemical dimerization of **TPA** through the active para positions.[20] These electrochemical results reveal that the encapsulation of **TPA** with peripheral fluorene moieties at all three of its para-phenyl positions efficiently blocks the electrochemically active sites of **TPA** and imparts enhanced electrochemical stability.

Figure 2 displays the room-temperature absorption and photoluminescence (PL) spectra of **TFTPA** recorded from a dilute dichloromethane solution and as a solid film on a quartz substrate. The two strong absorption bands at ca. 267 and

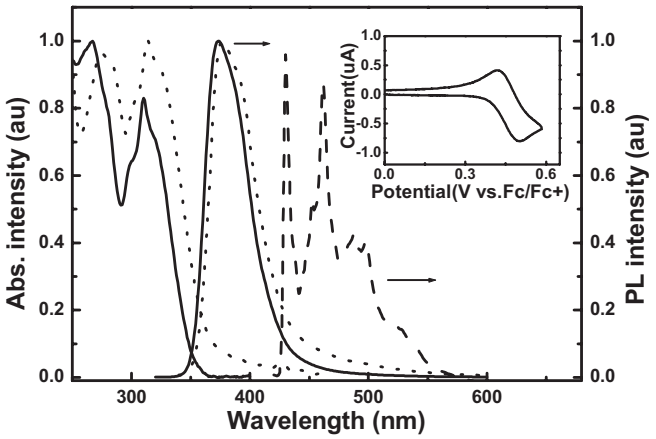

Figure 2. Room-temperature UV-vis absorption and PL spectra of **TFTPA** in dilute dichloromethane solution (solid lines) and in the solid state (dotted lines); 77 K phosphorescence spectra of **TFTPA** in 2-methyltetrahydrofuran solution (dashed line). The inset displays the cyclic voltammogram of **TFTPA** in CH_2Cl_2 solution.

310 nm arose mainly from the absorptions of the fluorene moieties and the **TPA** core, respectively. The **TFTPA** film exhibited PL in the near-UV region with a peak at 377 nm, which was slightly red-shifted (ca. 4 nm) when compared with that obtained from the dichloromethane solution. The small spectral shift in the solid state spectra suggests that any intermolecular interactions are weak,, i.e., they were restrained effectively by the bulky fluorene peripheries. The fluorescence quantum yield in dilute cyclohexane solution was 0.07 [using 9-phenyl-9*H*-carbazole ($\Phi_f = 0.33$) as the reference].[21] Figure 2 also depicts the phosphorescence spectra of **TFTPA** measured from a frozen 2-methyltetrahydrofuran matrix at 77 K. The highest-energy 0–0 phosphorescent emission located at 2.89 eV was used to calculate the triplet energy gap of **TFTPA**, giving a value higher than that reported for the common triplet blue-emitter FIrpic (2.62 eV). Using host materials that possess high triplet energies is a provision for effective confinement of the triplet excitons on the guest and, consequently, for prevention of back energy transfer between the host and dopant molecules.[8,22,23] In this case, the triplet energy of **TFTPA** is sufficiently high to serve as a decent host for short-wavelength dopants, such as FIrpic, and other long-wavelength dopants.

2.3. Electroluminescence Properties of LED Devices

To evaluate the utility of **TFTPA** as a host material, we fabricated blue-, green-, and red-electrophosphorescent device systems using FIrpic, $Ir(ppy)_3$, and $Ir(piq)_2acac$ as emitters, respectively, co-evaporated with the host material **TFTPA**. The typical multilayer architecture consisted of indium tin oxide (ITO)/4,4′-bis[*N*-(1-naphthyl)-*N*-phenylamino]biphenyl (NPB) (30 nm)/**TFTPA**: X (X = 7–21) wt % of dopant (40 nm)/1,3,5-tris(*N*-phenylbenzimidazol-2-yl)benzene (TPBI) (40 nm)/Mg:Ag (100 nm)/Ag (100 nm); the fabrication of these EL devices—through sequential vapor deposition of the materials onto ITO glass under vacuum (3×10^{-6} Torr)—and their characterization were similar to techniques we have reported previously.[24] In these devices, NPB and TPBI were employed as the hole-transporting layer (HTL) and the electron-transporting layer (ETL), respectively. For comparison, we also fabricated the corresponding blue-emitting control devices using mCP as the host material and FIrpic as the dopant at different doping concentrations (7 and 21 wt %). Figure 3 presents the EL characteristics of the three different color devices (R-G-B); the blue, green, and red emissions originated from the FIrpic, $Ir(ppy)_3$, and $Ir(piq)_2acac$ triplet emitters, respectively. The

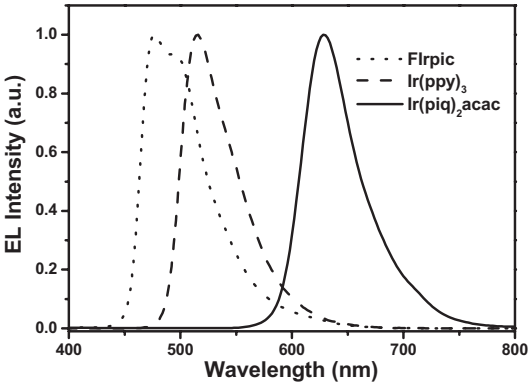

Figure 3. EL spectra of the blue-, green-, and red-emitting devices incorporating FIrpic, $Ir(ppy)_3$, and $Ir(piq)_2acac$ as emitters, respectively, co-evaporated with the host material **TFTPA**; the applied potential was 9 V.

CIE coordinates of these devices were located at (0.17, 0.37) for the blue-emitting device, (0.26, 0.66) for the green-emitting device, and (0.68, 0.32) for the red-emitting device.

Figure 4a displays the dependence of the voltage (V) on the current density (I) and brightness (L) for the blue-emitting devices containing various FIrpic concentrations. These devices exhibit rather low turn-on voltages (ca. 3 V, corresponding to a brightness of 1 cd m^{-2}), with the operating voltages being reduced slightly as the doping concentration increased. With respect to the doping concentration (from 7 to 21 wt %), the brightness of these devices improved as the concentration of the dopant (FIrpic) increased; the peak brightness of the 21-wt %-doped blue-emitting device reached as high as 70 394 cd m^{-2} at 13 V (650 mA cm^{-2}). According to the plots of external quantum efficiency and power efficiency versus current density (Fig. 4b), the device efficiency improved dramatically when the dopant concentration increased from 7 to 21 wt %. The maximum external quantum efficiency (max. η_{ext}) and maximum power efficiency (max. η_p) of the 21-wt %-doped blue-emitting device were 13.1 % (29.4 cd A^{-1}, 2.29 mA cm^{-2}) and 18.1 lm W^{-1}, respectively. These values are much higher than those of the control device (mCP doped with 21 wt % FIrpic), which displayed values of max. η_{ext} and max. η_p of 6.7 % and 6.3 lm W^{-1}, respectively. Note that the efficiencies of our **TFTPA**-based devices at a practical brightness of 100 cd m^{-2} remained above 12 % (26 cd A^{-1}) and 18 lm W^{-1}, which are among the highest levels ever reported for blue elec-

ADVANCED FUNCTIONAL MATERIALS

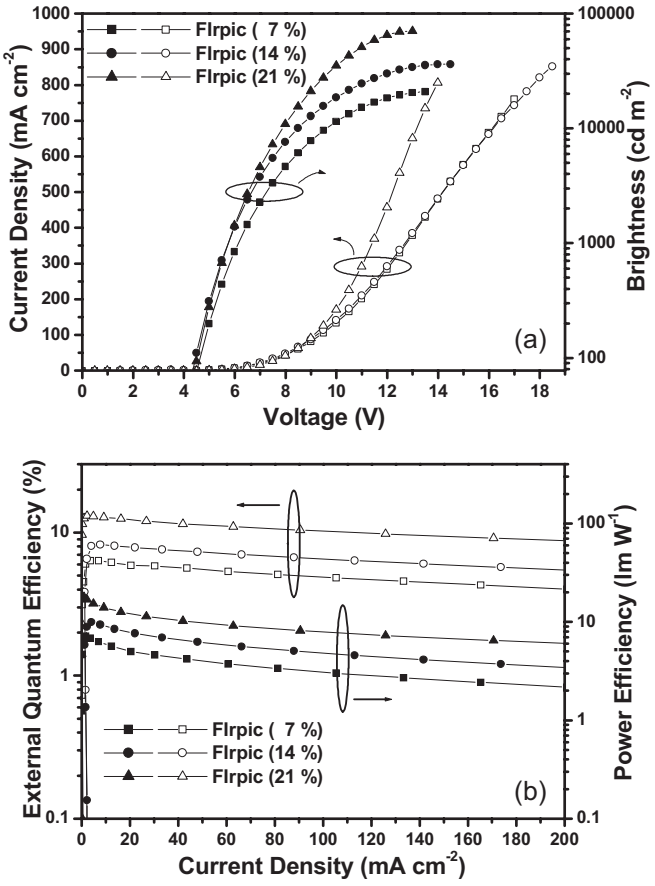

Figure 4. a) Current density (open symbols) and brightness (solid symbols) plotted as a function of the voltage and b) the external quantum efficiency and power efficiency plotted with respect to the current density for the FIrpic-doped **TFTPA** devices at various doping concentrations.

trophosphorescent devices;[9,10,22,25] even when the brightness was increased up to 1000 cd m^{-2}, the corresponding power efficiency remained above 16 lm W^{-1}. Table 1 lists the key characteristics of these phosphorescent devices.

In contrast to the **TFTPA**-based devices, the device efficiency of the control mCP-based devices improved only slightly as the dopant concentration increased; the performance of the 7 wt % FIrpic-doped mCP device exhibited values of max. η_{ext} and max. η_p of 6.7 % and 4.3 lm W^{-1}, respectively, which are quite comparable to those of the 21-wt %-doped device. This phenomenon may be attributed to triplet-triplet annihilation and concentration quenching arising from strong bimolecular interactions of the phosphor at high doping levels when mCP was used as the host material.[2,4,26] In the case of **TFTPA**, we speculate that the degree of aggregation between the triplet emitters may have been reduced significantly; consequently, self-quenching of the iridium phosphor was effectively restrained in the **TFTPA**-based devices. Figure 5 presents AFM topographic images of 21-wt %-FIrpic-doped films prepared using **TFTPA** and mCP as host materials. The topographic image of the **TFTPA**-based film indicates that no phase separation occurred; the root-mean-square surface roughness of this blend was 0.33 nm. In contrast, the mCP-based film displayed some hill-like patterns; its root-mean-square surface roughness was 0.63 nm (0.33 nm for the neat film, vide ante), which is almost twice that of the **TFTPA** blend. These AFM images suggest that the rigid cardo structure of **TFTPA** may provide an almost ideal stabilizing environment in which the phosphorescent emitters are isolated and dispersed homogeneously. Therefore, self-quenching arising from aggregation was almost negligible in the **TFTPA** host, with the resultant blue-emitting devices yielding a greater improvement in device efficiency at high dopant levels than did the mCP-based devices.

Figure 6a displays the dependence of the voltage (V) on the current density (I) and brightness (L) for the green-emitting devices at various doping levels of the green emitter Ir(ppy)$_3$. Again, the driving voltage reduced remarkably when the doping concentration was increased from 7 to 21 wt %. This result is similar to that of the blue-emitting device system described above. In addition, we also observed a gradual improvement in the brightness as the concentration of Ir(ppy)$_3$ increased. Figure 6b displays the external quantum efficiency and power efficiency plotted against the current density of these Ir(ppy)$_3$-based devices incorporating **TFTPA** as the host. The performance of these devices improved upon increasing the Ir(ppy)$_3$ concentration. The maximum values of η_{ext} and η_p of the 21-wt %-doped device were 12.0 % (44.1 cd A^{-1}, 11.5 mA cm^{-2}) and 21.0 lm W^{-1}, respectively; these efficiency characteristics are comparable to those of the Ir(ppy)$_3$-based devices incorporating CBP as the host material at the optimized dopant concentration (ca. 7 wt %) and with a similar device configuration.[27]

Figure 7 provides the current–voltage–brightness (I–V–L) characteristics, external quantum efficiencies, and power effi-

Table 1. Summary of device performance.

Device	FIrpic-doped TFTPA	Ir(ppy)$_3$-doped TFTPA	Ir(piq)$_2$acac-doped TFTPA	FIrpic-doped mCP
Dopant concentration	21 wt %	21 wt %	21 wt %	21 wt %
Voltage (V)[a]	3.1	3.5	2.6	4.1
Brightness (cd m^{-2})[b,c]	5526 (22875)	8592 (36837)	1945 (8663)	2819 (12004)
E.Q.E. (%)[b,c]	12.3 (10.2)	11.8 (10.1)	9.2 (8.1)	6.5 (5.6)
L.E. (cd A^{-1}) [b,c]	27.8 (23.0)	43.0 (36.9)	9.8 (8.7)	14.1 (12.0)
P.E. (lm W^{-1}) [b,c]	12.2 (7.9)	15.6 (10.3)	6.0 (3.9)	5.5 (3.7)
J (mA cm^{-2}) [d]	3.4	2.4	10.1	7.1
Max brightness (cd m^{-2})	70394 (@ 13 V)	145641 (@ 16 V)	34973 (@ 14 V)	35250 (@ 15 V)
Max E.Q.E. (%)	13.1	12.0	9.6	6.7
Max L.E. (cd A^{-1})	29.4	44.1	10.2	14.5
Max P.E. (lm W^{-1}) [e]	18.1 (93.4)	21.0 (1247)	9.0 (71)	6.3 (730)
EL λ_{max} (nm) [f]	478	516	624	478
CIE, x and y [f]	0.17 and 0.39	0.26 and 0.66	0.68 and 0.32	0.15 and 0.37

[a] Recorded at 1 cd m^{-2}. [b] Recorded at 20 mA cm^{-2}. [c] The data in parentheses were recorded at 100 mA cm^{-2}. [d] Current density at the brightness of 1000 cd m^{-2}. [e] The data in parentheses were the corresponding brightness (cd m^{-2}). [f] At 9 V.

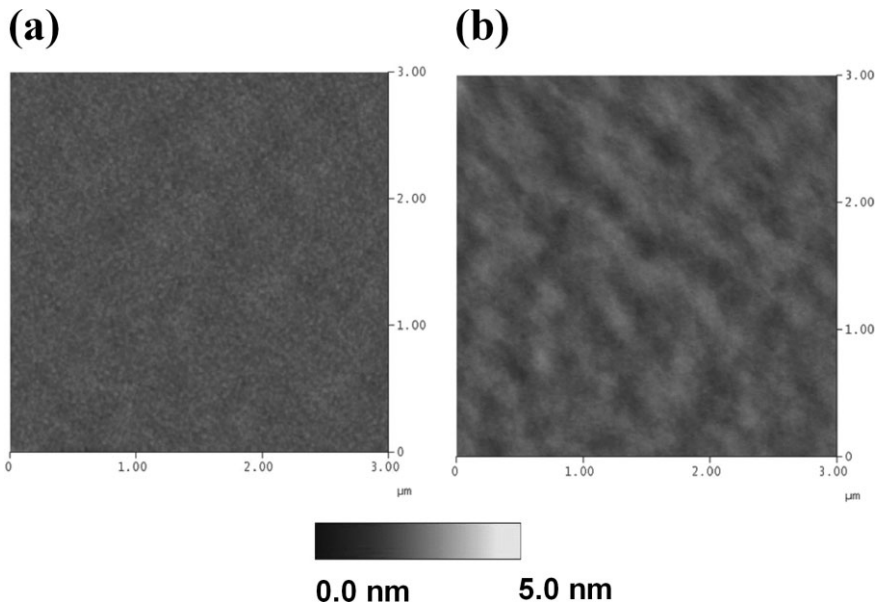

Figure 5. AFM topographic images (tapping mode) of the 21%-FIrpic-doped a) TFTPA and b) mCP films. Films were vapor-deposited onto silicon wafers under vacuum.

ciencies of the $Ir(piq)_2acac$-based red-emitting devices. Similar to the behavior of the green-emitting devices, increasing the dopant concentration significantly reduced the turn-on voltage, accompanied by a large enhancement in efficiency. The 21-wt%-doped device exhibited the highest performance with an extremely low turn-on voltage (ca. 2.6 V); the maximum values of η_{ext} and η_p reached as high as 9.6% (10.2 cd A^{-1}, 2.75 mA cm^{-2}) and 9.0 lm W^{-1}, respectively. We note that the peak power efficiency of the **TFTPA**-based device was approximately three times higher than that of the CBP-based devices (ca. 3 lm W^{-1}) at the optimized dopant concentration (ca. 7 wt%).[28] Furthermore, our red-emitting devices exhibited a much reduced degree of efficiency roll-off at high brightness. The external quantum efficiency and power efficiency of our 21-wt%-$Ir(piq)_2acac$-doped

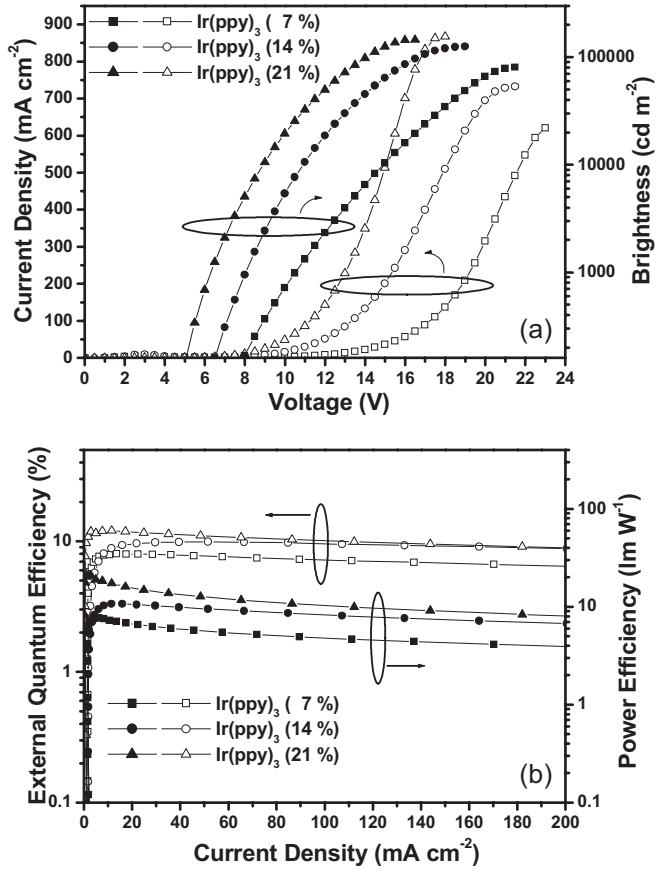

Figure 6. a) Current density (open symbols) and brightness (solid symbols) plotted as a function of the voltage and b) the external quantum efficiency and power efficiency plotted as a function of the current density for the $Ir(ppy)_3$-doped **TFTPA** devices at various doping concentrations.

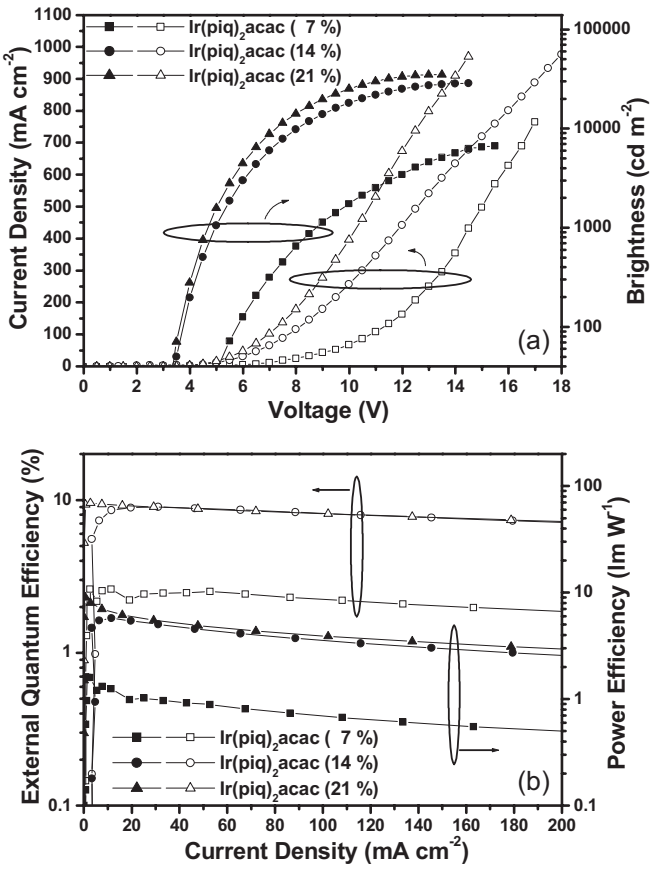

Figure 7. a) Current density (open symbols) and brightness (solid symbols) plotted as function of the voltage and b) the external quantum efficiency and power efficiency plotted as a function of the current density for the $Ir(piq)_2acac$-doped **TFTPA** devices at various doping concentrations.

ADVANCED FUNCTIONAL MATERIALS

TFTPA device at 100 cd m^{-2} were 9.3 % and 8.8 lm W^{-1}, respectively; when we increased the brightness of this device up to the order of 1×10^3 cd m^{-2}, the corresponding EL efficiencies remained above 9.2 % and 6.6 lm W^{-1}, respectively, which are among the best reported to date for red-emitting electrophosphorescent devices based on $Ir(piq)_2acac$ and its analogues.[29–31]

According to the *I–V* curve characteristics of the above three different color (R-G-B) device systems, an increase in the dopant concentration led to a decreasing drive voltage. This phenomenon indicates that the charges may be injected directly to the dopant molecules at high doping concentrations; these moieties then serve as an additional channel to transport charges by hopping between the dopant sites, with **TFTPA** acting as an inert host matrix.[5,32–35] In addition, when the dopant concentration is increased, the opportunity for carrier recombination at the dopant emitters might also increase, leading to a higher device efficiency. Consequently, we speculate that the pronounced enhancement of the device power efficiency at high doping concentrations arose from two contributing factors: the increased luminous efficiency and the lowered driving voltage. More importantly, the excellent performances of these blue-, green-, and red-emitting devices were obtained from simple device architectures, which make them very attractive for commercial applications.

3. Conclusions

We have developed a facile synthetic route for the preparation of a novel host material, **TFTPA**, which contains a **TPA** core with three 9-phenyl-9-fluorenyl groups attached at its peripheries. This one-step Friedel–Crafts-type reaction is not only simple but, because of the use of inexpensive reactants and mild operating conditions, it is also cost effective. Using this synthetic strategy, **TFTPA** can be produced readily on a large scale. Owing to the presence of the sterically bulky 9-phenyl-9-fluorenyl groups, **TFTPA** exhibits a high glass transition temperature (186 °C) and is morphologically and electrochemically stable. AFM measurements suggested that the aggregation of the triplet iridium dopant was depressed significantly when **TFTPA** was used as the host. As a result, self-quenching is effectively reduced leading to highly efficient phosphorescent devices at high dopant concentrations (optimized at 21 wt %). The performance of the **TFTPA**-based devices is far superior to those of the corresponding mCP- or CBP-based devices, particularly in the blue- and red-emitting electrophosphorescent device systems. The efficiencies of the blue-emitting device reached 12 % (26 cd A^{-1}) and 18 lm W^{-1} at a practical brightness of 100 cd m^{-2}; these values are among the highest ever reported for blue electrophosphorescent devices. In addition, the red-emitting device exhibited an extremely low turn-on voltage (2.6 V) and a threefold enhancement in the power efficiency (9.0 lm W^{-1}) relative to those of reference devices based incorporating CBP as the host material. As well as yielding highly efficient full-color phosphorescence, our present approach should be attractive for the development of commercial applications because the simple device structure promises low-cost manufacturing.

4. Experimental

General Procedures: ^1H and ^{13}C NMR spectra were recorded on a Bruker-DRX 300 (300 MHz) spectrometer. Mass spectra were obtained using a Finnigan/Thermo Quest MAT 95XL mass spectrometer. Differential scanning calorimetry (DSC) was performed using a Seiko Exstar 6000DSC instrument operated at heating and cooling rates of 20 and 40 °C min^{-1}, respectively. Samples were scanned from 30 to 420 °C, cooled to 0 °C, and then heated again to 420 °C; the glass transition temperature (T_g) was determined from the second heating scan. Thermogravimetric analysis (TGA) was undertaken using a DuPont TGA 2950 instrument. The thermal stability of the samples under a nitrogen atmosphere was determined by measuring their mass loss while heating at a rate 20 °C min^{-1}. UV-vis spectra were measured using an HP 8453 diode-array spectrophotometer. PL spectra were obtained using a Hitachi F-4500 luminescence spectrometer. Cyclic voltammetry (CV) measurements were performed using a BAS 100 B/W electrochemical analyzer operated at a scan rate of 100 mV s^{-1}; the samples were dissolved in anhydrous CH_2Cl_2 containing 0.1 M tetrabutylammonium hexafluorophosphate ($TBAPF_6$) as the supporting electrolyte. The potentials were measured against an Ag/Ag^+ (0.01 M $AgNO_3$) reference electrode, using ferrocene as the internal standard. Atomic force microscopy measurements were performed in the tapping mode under ambient conditions using a Digital Nanoscope IIIa instrument.

Tris[4-(9-phenylfluoren-9-yl)phenyl]amine (TFTPA): CF_3SO_3H (1.64 g, 10.9 mmol) was added dropwise at 25 °C under a nitrogen atmosphere to a solution of triphenylamine (1.00 g, 4.08 mmol) and 9-phenyl-9-fluorenol (3.26 g, 12.6 mmol) in 1,4-dioxane (50 mL). The mixture was stirred under nitrogen at 80 °C; as the reaction proceeded, a white precipitate appeared because of the insolubility of **TFTPA**. After 3 h, the mixture was cooled to room temperature; the precipitate was filtered, washed with acetone (2 × 25 mL), and dried to provide a crude product, which was purified by repeated (two times) vacuum sublimation to yield ultrapure **TFTPA** as a white solid (3.9 g, 72.0 %). ^1H NMR ($CDCl_3$, 300 MHz): δ 7.79 (d, J = 7.5 Hz, 6H), 7.36–7.45 (m, 12H), 7.23–7.33 (m, 21H), 7.05 (d, J = 8.6 Hz, 6H), 6.89 (d, J = 8.6 Hz, 6H). ^{13}C NMR ($CDCl_3$, 75 MHz): δ151.3, 146.0, 145.8, 140.0, 139.7, 128.8, 128.1, 128.0, 127.6, 127.4, 126.5, 126.2, 123.5, 120.1, 64.9. HRMS $[M+H]^+$: calcd. for $C_{75}H_{52}N$ 966.4101, found 966.4106. Anal. Calcd. for $C_{75}H_{51}N$: C, 93.23; H, 5.32; N, 1.45. Found: C, 92.91; H, 5.46; N, 1.40.

Received: February 14, 2007
Revised: April 11, 2007
Published online: August 28, 2007

[1] T. Fuhrmann, J. Salbeck, *MRS Bull.* **2003**, *28*, 354.
[2] M. A. Bado, D. F. O'Brien, Y. You, A. Shoustikov, S. Sibley, M. E. Thompson, S. R. Forrest, *Nature* **1998**, *395*, 151.
[3] S. Lamansky, P. Djurovich, D. Murphy, F. Abdel-Razzaq, H. E. Lee, C. Adachi, P. E. Burrows, S. R. Forrest, M. E. Thompson, *J. Am. Chem. Soc.* **2001**, *123*, 4304.
[4] N. J. Turro, *Modern Molecular Photochemistry*, University Science Books, Sausalito, CA **1991**.
[5] C. Adachi, M. A. Baldo, M. E. Thompson, S. R. Forrest, *J. Appl. Phys.* **2001**, *90*, 5048.
[6] Y. Kawamura, K. Goushi, J. Brooks, J. J. Brown, H. Sasabe, C. Adachi, *Appl. Phys. Lett.* **2005**, *86*, 071 104.
[7] M. H. Tsai, Y. H. Hong, C. H. Chang, H. C. Su, C. C. Wu, A. Matoliukstyte, J. Simokaitiene, S. Grigalevicius, J. V. Grazulevicius, C. P. Hsu, *Adv. Mater.* **2007**, *19*, 862.
[8] R. J. Holmes, S. R. Forrest, Y.-J. Tung, R. C. Kwong, J. J. Brown, S. Garon, M. E. Thompson, *Appl. Phys. Lett.* **2003**, *82*, 2422.

[9] S.-J. Yeh, M.-F. Wu, C.-T. Chen, Y.-H. Song, Y. Chi, M.-H. Ho, S.-F. Hsu, C. H. Chen, *Adv. Mater.* **2005**, *17*, 285.
[10] M.-H. Tsai, H.-W. Lin, H.-C. Su, T.-H. Ke, C.-C. Wu, F.-C. Fang, Y.-L. Liao, K.-T. Wong, C.-I. Wu, *Adv. Mater.* **2006**, *18*, 1216.
[11] K. Brunner, A. van Dijken, H. Borner, J. J. A. M. Bastiaansen, N. M. M. Kiggen, B. M. W. Langeveld, *J. Am. Chem. Soc.* **2004**, *126*, 6035.
[12] T. F. Palmer, S. S. Parmar, *J. Photochem.* **1985**, *31*, 273.
[13] C.-L. Chiang, C.-F. Shu, *Chem. Mater.* **2002**, *14*, 682.
[14] H. Z. Xie, M. W. Liu, O. Y. Wang, X. H. Zhang, C. S. Lee, L. S. Hung, S. T. Lee, P. F. Teng, H. L. Kwong, H. Zheng, C. M. Che, *Adv. Mater.* **2001**, *13*, 1245.
[15] S. Chew, C. S. Lee, S. T. Lee, P. Wang, J. He, W. Li, J. Pan, X. Zhang, H. Kwong, *Appl. Phys. Lett.* **2006**, *88*, 093 510.
[16] T. Ohta, K. Shudo, T. Okamoto, *Tetrahedron Lett.* **1983**, *24*, 71.
[17] K.-T. Wong, Z.-J. Wang, Y.-Y. Chien, C.-L. Wang, *Org. Lett.* **2001**, *3*, 2285.
[18] P.-I. Shih, C.-L. Chiang, A. K. Dixit, C.-K. Chen, M.-C. Yuan, R.-Y. Lee, C.-T. Chen, E. W.-G. Diau, C.-F. Shu, *Org. Lett.* **2006**, *8*, 2799.
[19] K. Katsuma, Y. Shirota, *Adv. Mater.* **1998**, *10*, 223.
[20] E. T. Seo, R. F. Nelson, J. M. Fritsch, L. S. Marcoux, D. W. Leedy, R. N. Adams, *J. Am. Chem. Soc.* **1966**, *88*, 3498.
[21] N. Nijegorodov, P. V. C. Luhanga, J. S. Nkoma, D. P. Winkoun, *Spectrochim. Acta Part A* **2006**, *64*, 1.
[22] S. Tokito, T. Iijima, Y. Suzuri, H. Kita, T. Tsuzuki, F. Sato, *Appl. Phys. Lett.* **2003**, *83*, 569.
[23] I. Tanaka, Y. Tabata, S. Tokito, *Chem. Phys. Lett.* **2004**, *400*, 86.
[24] F.-I. Wu, P.-I. Shih, M.-C. Yuan, A. K. Dixit, C.-F. Shu, Z.-M. Chung, E. W.-G. Diau, *J. Mater. Chem.* **2005**, *15*, 4753.
[25] P. A. Vecchi, A. B. Padmaperuma, H. Qiao, L. S. Sapochak, P. E. Burrows, *Org. Lett.* **2006**, *8*, 2799.
[26] M. A. Baldo, C. Adachi, S. R. Forrest, *Phys. Rev. B* **2000**, *62*, 10 967.
[27] M. A. Baldo, S. Lamansky, P. E. Burrows, M. E. Thompson, S. R. Forrest, *Appl. Phys. Lett.* **1995**, *75*, 4.
[28] Y. J. Su, H. L. Huang, C. L. Li, C. H. Chien, Y. T. Tao, P. T. Chou, S. Datta, R. S. Liu, *Adv. Mater.* **2003**, *15*, 884.
[29] A. Tsuboyama, H. Iwawaki, M. Furugori, T. Mukaide, J. Kamatani, S. Igawa, T. Moriyama, S. Miura, T. Takiguchi, S. Okada, M. Hoshino, K. Ueno, *J. Am. Chem. Soc.* **2003**, *125*, 12 971.
[30] C. H. Yang, C. C. Tai, I. W. Sun, *J. Mater. Chem.* **2004**, *14*, 947.
[31] X. Yang, D. C. Müller, D. Neher, K. Meerholz, *Adv. Mater.* **2006**, *18*, 948.
[32] Y. L. Tung, S. W. Lee, Y. Chi, L. S. Chen, C. F. Shu, F. I. Wu, A. J. Carty, P. T. Chou, S. M. Peng, G. H. Lee, *Adv. Mater.* **2005**, *17*, 1059.
[33] Y. Y. Noh, C. L. Lee, J. J. Kim, *J. Chem. Phys.* **2003**, *118*, 2853.
[34] R. J. Holmes, B. W. D'Andrade, S. R. Forrest, X. Ren, J. Li, M. E. Thompson, *Appl. Phys. Lett.* **2003**, *83*, 3818.
[35] Y. L. Tung, L. S. Chen, Y. Chi, P. T. Chou, Y. M. Cheng, E. Y. Li, G. H. Lee, C. F. Shu, F. I. Wu, A. J. Carty, *Adv. Funct. Mater.* **2006**, *16*, 1615.